ACADEMIC PRESS

Available online at www.sciencedirect.com

SCIENCE DIRECT®

Journal of Magnetic Resonance 162 (2003) 206–216

JMR Journal of Magnetic Resonance

www.elsevier.com/locate/jmr

The DIVAM sequence: selective excitation of signals from both rigid and mobile domains in a fluoropolymer

Paul Hazendonk,[a,*] Robin K. Harris,[b] Shinji Ando,[c] and Paolo Avalle[b]

[a] *Department of Chemistry and Biochemistry, University of Lethbridge, 4401 University Drive W., Lethbridge, Alta., Canada T1K 3M4*
[b] *Department of Chemistry, University of Durham, South Road, Durham DH1 3LE, UK*
[c] *Department of Organic and Polymeric Materials, Tokyo Institute of Technology, Ookayama, Meguro-ku, Tokyo 152-8552, Japan*

Received 17 September 2002; revised 23 January 2003

Abstract

Simulations have been carried out on *z*-magnetizations produced by (and hence of the resulting spectra from) the dipolar filter (DF) and the recently suggested "Discrimination Induced by Variable-Amplitude Minipulses" (DIVAM) pulse sequences [S. Ando et al., Polymer 42 (2001) 8137; Magn. Reson. Chem. 40 (2002) 97]. The strengths of dipolar interactions have been modelled by introducing different values for transverse relaxation times. The DF case has been extended by allowing the pulse angles to be smaller than 90°. The pulse intervals have also been used as variables. For the DIVAM case, the variables are similarly the minipulse nutation angles and minipulse intervals. The computations show that DIVAM is superior to DF in terms of selectivity for spectra of heterogeneous materials such as semi-crystalline polymers. The effects of the pulse sequences on ^{19}F spectra of poly(vinylidene fluoride) (PVDF) and of a copolymer of vinylidene fluoride and trifluoroethylene (p(VDF/TrFE)) are presented, together with fits of the experimental results by the simulations.

Keywords: DIVAM; Dipolar filter; Crystalline domain; Amorphous domain; Simulation; Fluoropolymers

1. Introduction

In NMR studies of heterogeneous polycrystalline materials, methods of selecting specifically for the spectrum of each constituent domain are desirable. Such selective excitation methods must be based on properties of nuclei unique to that domain [1,2], for instance on differences in relaxation, shielding, or the strength of dipolar coupling interactions.

Polymeric materials, such as poly(vinylidene fluoride) (PVDF), are semi-crystalline, with domains characterized by being either relatively mobile (amorphous) or relatively rigid (crystalline). There is usually significant spectral overlap of signals corresponding to these domains (especially for proton NMR), leaving selective methods to be based largely on relaxation and dipolar coupling behaviour. Consequently, most work has been limited to methods such as dipolar dephasing [1,3], dipolar filter (DF), cross-polarization (CP), and T_1 or $T_{1\rho}$ filters.

The DF [1,4,5] and Dipolar Dephasing (DD) [3,6] experiments exploit differences in heteronuclear dipolar interaction strengths between the domains. Dipolar dephasing achieves selectivity by delaying heteronuclear decoupling (usually following CP) for a brief period before acquiring the signal of the observed nuclide (see Fig. 1(a)). Since in a rigid (crystalline) domain dipolar interactions are not substantially averaged by random motion, they tend to be characterized by strong dipolar interactions, and consequently the corresponding signal dephases much more rapidly than the magnetization of a mobile domain during the delayed decoupling or delayed acquisition period.

The DF (Figs. 1(b) and 2(a)) achieves similar filtration through a pulse train of 90° pulses that refocuses homonuclear dipolar couplings, and also chemical shift anisotropy terms. The spacing between the pulses determines the effective timescale, and hence the effective coupling strength, that is refocused. Strong dipolar in-

* Corresponding author. Fax: +1-403-329-2657.
E-mail address: paul.hazendonk@uleth.ca (P. Hazendonk).

1090-7807/03/$ - see front matter © 2003 Elsevier Science (USA). All rights reserved.
doi:10.1016/S1090-7807(03)00048-X

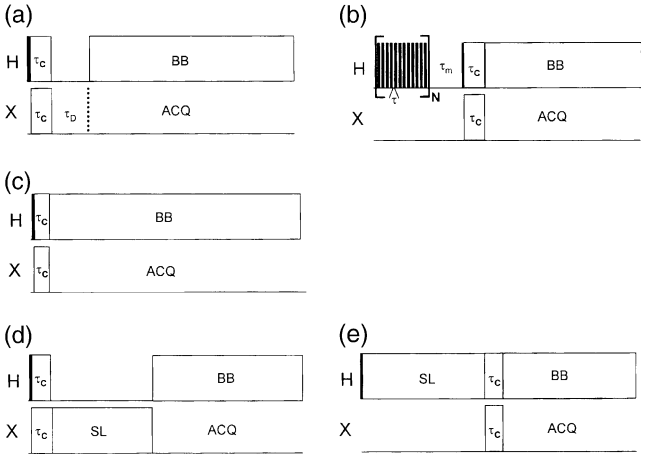

Fig. 1. Pulse sequences involved in the present work, all involving CP from ^{1}H to another nuclide, X: (a), Dipolar dephasing (DD); (b), Dipolar filter (DF) (all pulses in the pulse train are 90°); (c), Simple CP; (d), X-nucleus $T_{1\rho}$-filter; (e), Proton $T_{1\rho}$-filter.

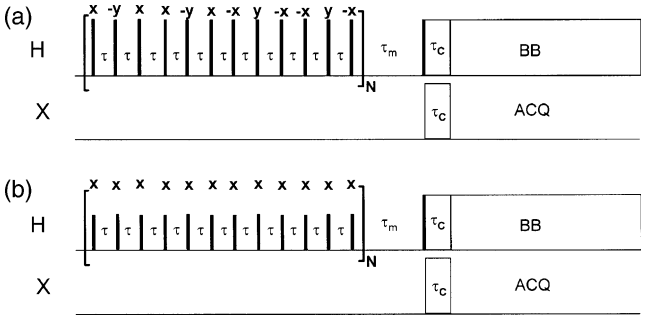

Fig. 2. (a) The DF pulse sequence, with CP. (All pulses in the pulse train are 90°, with the phases as indicated above.) (b) The DIVAM pulse sequence, with CP. (The pulse angle is variable but the phase is fixed as indicated above.)

teractions are not refocused, or are refocused a lot less efficiently than weak dipolar terms, leading to selection dependent on average dipolar coupling strength. One drawback of both DD and DF approaches to selection is that it is not feasible to adjust the conditions so as to select specifically for strong dipolar interactions. These methods can only be used to select for the mobile (amorphous) domains.

The Hartmann–Hahn CP technique (shown in Fig. 1(c)) can also used to discriminate between domains on the basis of the CP rate, again relying on variations in the strengths of dipolar interactions [7]. CP can be selective for domains with strong dipolar interactions when very short contact periods are used (because CP rates are high in such cases) but it cannot normally select for relatively mobile domains.

Relaxation filters, as seen in Fig. 1(d), exploit differences in the relaxation rates for the two types of domains. The most common filters are based on rotating frame relaxation times, where one can choose the time scale based on relaxation efficiency at the spin-locking power applied.

The DIVAM pulse sequence (Discrimination Induced by Variable-Amplitude Minipulses) was introduced in 2001 [8,9], but its operation has not so far been analysed in detail. The version used in these publications (and for the experimental results described herein) is shown in Fig. 2(b). It consists of a series of minipulses separated by evolution intervals, each of duration τ. The key variable (apart from τ) is the nutation angle, θ, induced by each minipulse and controlled by either the amplitude or the duration of the pulses. In principle, any number, N of such minipulses may be used. At the end of the pulse train, the direction of the magnetization will depend on N and θ and on both coherent and incoherent dephasing processes that occur during the times τ. The dephasing will also influence the magnitude of the magnetization. In principle, of course, there will also be effects from the influence of T_1 and from the degree of off-resonance during the experiment. However, in general T_1 for solids will be significantly longer than $N\tau$, and consequently this factor will be ignored herein. Moreover, we will concentrate initially on the on-resonance situation in this article.

The sequence is capable of selectively providing spectra of amorphous and crystalline phases of semicrystalline polymers because the extent of dephasing during the minipulse intervals will depend on transverse relaxation rates and hence on the strengths of dipolar coupling in the domains. In that sense, it is related to the DF sequence, though its mode of operation is very different. It can also be thought of as having analogies to DANTE excitation, or as a modification of the Goldman–Shen pulse sequence since it selects on the basis of dephasing in the transverse plane [1]. There will be a balance between the effects of θ and dephasing which, in general, will lead to an accumulation of θ, producing net magnetization at some total nutation angle θ_t in the yz plane at the end of the series of minipulses as illustrated in Fig. 3. The transverse component of this magnetization may be detected directly and will clearly be at an optimum for $\theta_t = 90°$. Alternatively, this transverse magnetization can be cross-polarised via a Hartmann–Hahn contact to a different nuclear species (e.g., if developed in ^{1}H it can be transferred to ^{19}F for detection in the case of a fluoropolymer), which may yield benefits in terms of chemical shift dispersion. However, as used in our previous publications [6,7], the minipulse train has been followed by a 90° pulse prior to Hartmann–Hahn contact, as shown in Fig. 2(b), which means that optimum (negative) signal is obtained for $\theta_t = 180°$. However, of greater significance is the fact that differences in transverse relaxation rates between two domains in a sample will result in different values of the net nutation angle θ_t. Thus, signals with rapid trans-

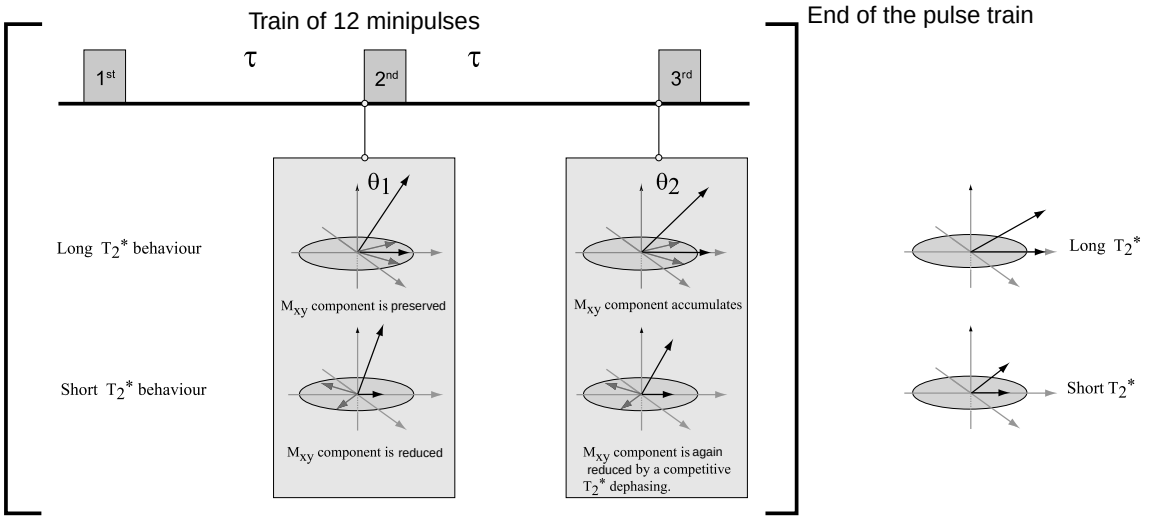

Fig. 3. Mode of operation of the DIVAM pulse sequence for the cases of short and long transverse relaxation times. The net magnetization vector and its component in the *xy* plane are displayed at various times in the sequence.

verse relaxation (strong dipolar interactions) will lag behind (in terms of θ_t) those characterized by slow relaxation (weak dipolar couplings). For semi-crystalline polymers these two cases will normally be for the crystalline and amorphous domains, respectively, when the sample temperature is higher than the glass transition temperature. The magnitude of the difference in θ_t (and the magnitudes of the magnetizations themselves) can be tuned by adjusting θ and τ (and in principle N). Of particular interest is the fact that, as the minipulse nutation angle increases (for a suitable choice of τ), the value of θ_t will approach 90° for each domain in turn, which implies that (after the CP pulse) one of the signals for the observed nuclide will pass through a null condition, leading to the appearance of a selective spectrum of the other domain. This null signal situation will be reached first for the domain with the longer transverse relaxation time, at which point the spectrum of the more rigid domain will be obtained, though generally with some intensity loss. It will be easier to obtain a high-intensity spectrum of the domain with the long transverse relaxation time (which

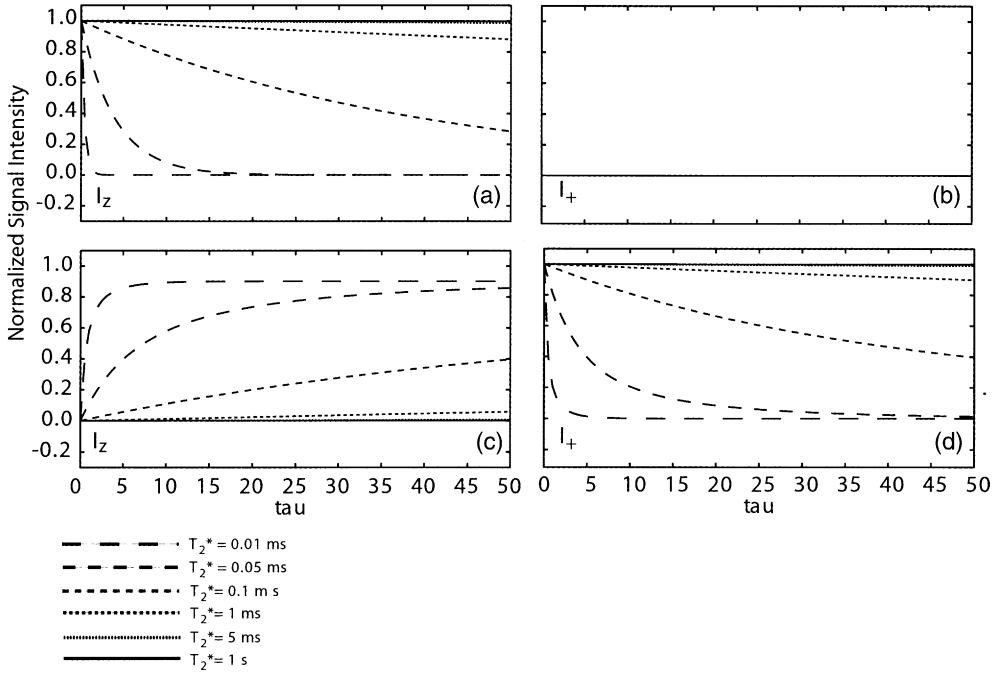

Fig. 4. Longitudinal (a and c) and transverse (b and d) magnetizations as a function of interpulse times, τ (μs), for the DF (a and b) and DIVAM (c and d) pulse sequences for several values of T_2^*. The longitudinal relaxation time is taken as 1 s and the minipulse nutation angle as 7.5°.

will in principle be negative) for somewhat larger minipulse nutation angles.

This paper discusses numerical simulations of the effects of the DIVAM sequence, showing how selectivity can be tuned to either the rigid or the mobile domain. Moreover, since a thorough analysis of the mode of operation of the DF pulse sequence does not appear to have been published hitherto, we report similar simulations for this sequence, and have extended the analysis to a range of pulse angles so as to make a comparison with DIVAM. Thus the minipulse angle and spacing were varied for both DIVAM and DF. However, we have limited our calculations to 12 minipulses for DIVAM (for equivalence to DF) and to $N = 1$.

2. Materials and methods

2.1. Solid-state NMR

The ^{19}F CPMAS NMR spectra of p(VDF/TrFE) were collected using a Chemagnetics CMX-200 spectrometer operating at 188.288 MHz for fluorine and 200.13 MHz for proton. A commercial Chemagnetics ^{1}H–^{19}F double-tuned APEX MAS probe capable of high power (ca. 100 kHz) heteronuclear decoupling and equipped with zirconia 4-mm-o.d. Pencil rotors (including Vespel drive tips and end-caps) was used. Samples were spun at the magic angle at rates of ca. 14–16 kHz.

The PVDF spectra were recorded on a Varian UNITY *Inova* spectrometer with a 7.05 T Oxford Instruments magnet equipped with a DOTY ^{1}H–^{19}F double-tuned MAS probe, with silicon nitride rotors (5 mm o.d.) and Aurum end-caps. The Larmor frequencies were 282.204 MHz for fluorine and 300 MHz for proton. The MAS rate was adjusted to 14 kHz.

Experimental conditions: proton 90° pulse 3.5 μs (*Inova*) (calibrations were performed on the 360° pulse determined to within 0.1 μs at 14.0 μs; thus the error should be considered to be of the order of 1% or approximately 1° for a 90° pulse), 3.1 μs (CMX); contact time 0.5 ms (*Inova*), 1 ms (CMX); recycle delay 4 s (*Inova*), 5 s (CMX) (much longer than the PVDF T_1 of 0.3 s,

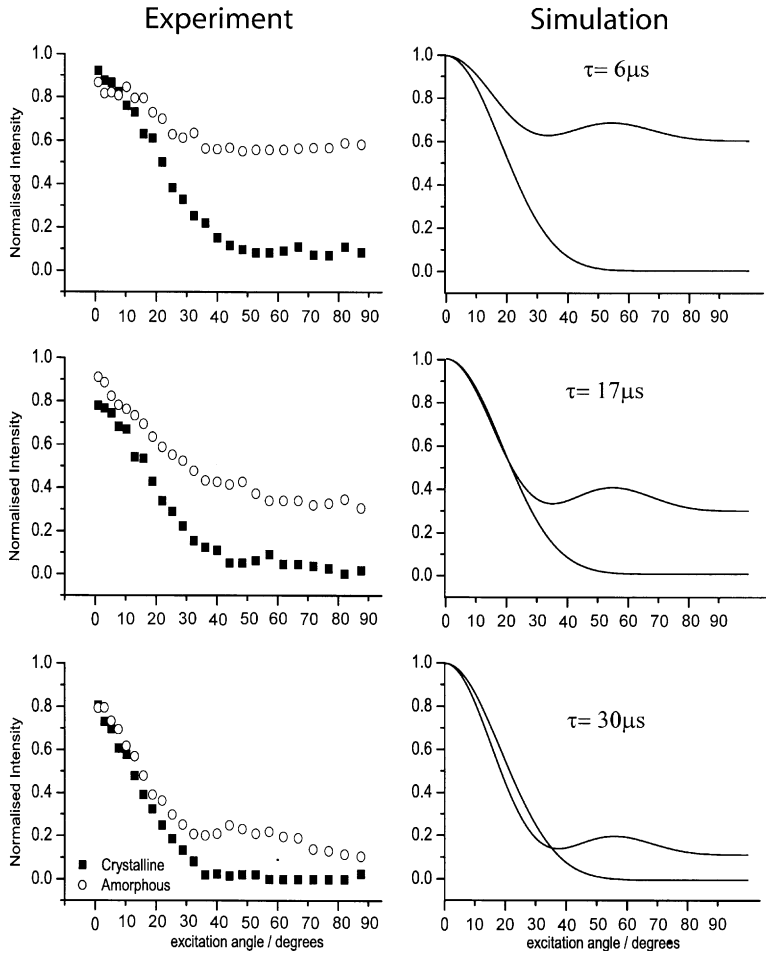

Fig. 5. Excitation behaviour of ^{19}F magnetizations for PVDF under the influence of the DF pulse sequence for three different values of the interpulse time and as a function of the minipulse nutation angle, θ. The values of T_1 are 0.3 s. The crystalline- and amorphous-phase values of T_2^* are 0.03 and 0.3 ms, respectively.

as measured by inversion recovery). The spin rate was 14 kHz (*Inova*), 15.5 kHz (CMX); number of transients 64 (*Inova*), 512 (CMX); proton decoupling field applied during acquisition equivalent to 71.43 kHz (*Inova*), 80 kHz (CMX). The minipulse power was calibrated to obtain the corresponding nutation angles, and then varied from the spectrometer control software. The range of nutation angles considered was between 3° and 88° (*Inova*), 5.5° to 90° (CMX). For both pulse sequences the nutation angle arrays were repeated for three different interpulse spacings ($\tau = 6$, 17, and 30 μs). The value of the parameter τ_m (Fig. 2) was set to be half of the interpulse spacing τ for all cases.

Experimental intensities were obtained by spectral deconvolution performed using Origin 6.1. Peak positions and linewidths were fixed throughout the array and only the intensities were allowed to vary. The lineshape was presumed to be Lorentzian throughout the analysis. As an additional constraint, both the areas and the widths of the two defects unit peaks (at −113 and −115 ppm, Fig. 9) were set to be equal. In this way the number of variables was reduced and the fitting of complicated spectra obtained by DIVAM (showing positive and negative peaks) was made possible.

For both spectrometers, unwanted background signal on the fluorine channel should be minimal since H → F CP was used. Also, to reduce the effects of RF inhomogeneity, the sample was restricted to the central part of the rotor (ca. 3.5 mm in length).

All experiments were carried out at room temperature and no attempt was made to compensate for heating due to sample spinning. Fluorine-19 chemical shifts are quoted with respect to the signal for $CFCl_3$, and were measured via a replacement sample of liquid C_6F_6 at −164 ppm. The Bloch–Siegert effect, which is a chemical shift displacement of ca. 1.4 ppm caused by the ^1H decoupling, was corrected by decoupling during the acquisition of the signal from the reference sample. The PVDF sample was purchased from Goodfellow (Cambridge, UK), and the p(VDF/TrFE) copolymer sample was obtained from Daikin Industries (Japan). The VDF content of p(VDF/TrFE) determined from ^{19}F solution NMR is 78 mol% and the melting temperature determined from a DSC thermogram (1st run) is 148 °C.

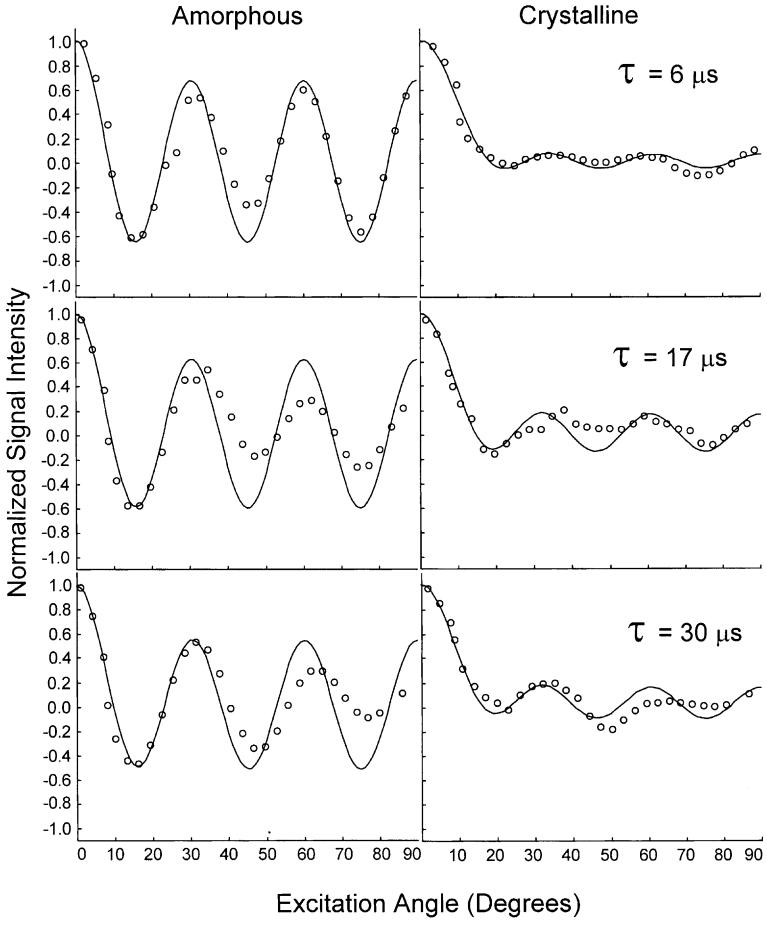

Fig. 6. Experimental plots of PVDF signal intensity for the DIVAM sequence of the two domains as a function of minipulse nutation angle for three separate values of the interpulse time. The solid lines show calculated variations using T_2^* of 0.02 ± 0.01 ms and 0.8 ± 0.4 ms for the crystalline and amorphous phases, respectively.

Samples were ground into powders under liquid nitrogen, dried under vacuum at 70 °C for 8 h and annealed at 110 °C for 72 h in order to evaporate absorbed water and volatile additives prior to being packed into the rotor.

2.2. Simulations

Density matrix calculations were carried out for a single-spin system employing the strong RF approximation for the pulses, and allowing for free evolution and relaxation during the pulse spacings. A simple Hamiltonian of the form $\mathbf{H} = \nu_o \mathbf{I}_z$ was used. The initial density matrix, $\mathbf{I}_z$, is propagated through time using the Liouvillian, $\mathbf{L} = i[\mathbf{H} \otimes \mathbf{I} - \mathbf{I} \otimes \mathbf{H}] + \mathbf{R}$, where $\mathbf{R}$ is assumed to be diagonal, with T_2^{*-1} defining a Lorentzian relaxation rate for the single-quantum coherences and T_1^{-1} for the z-magnetization. Transverse relaxation is considered to model the effects of dipolar coupling. This simulation corresponds to the classical description of a single spin subjected to sequential rotation and precession–relaxation periods.

The minipulse sequences were implemented with phase cycles $(x, -y, x, x, -y, x, -x, y, -x, -x, y, -x)$ and $(x, x, x, x, x, x, x, x, x, x, x, x)$ for the DF and DIVAM cases, respectively, as in Fig. 2. A 12-pulse train was used in each case (with $N = 1$). The minipulse angle, θ, pulse spacing, τ, offset from resonance, ν_o, and transverse and longitudinal relaxation times, T_2^* and T_1, were input parameters. The z-magnetization at the end of the pulse train (which is directly proportional to the fluorine signal observed after CP) was computed either as a function of the pulse spacing τ or excitation angle θ, for various values of T_2^*.

All simulations were performed in the MATLAB programming environment on a standard PC with a 500 MHz P3 processor.

3. Results and discussion

As indicated above, simulations of the DF and DIVAM pulse sequences were performed for the on-resonance situation over a range of transverse relaxation times, as a function of the pulse spacing τ. Fig. 4 shows the remaining z-magnetization (a and c) and any emerging transverse magnetization (b and d) after the DIVAM and DF pulse trains, with variation of the pulse spacing from 0 to 50 μs for spin–spin relaxation times ranging from 10 μs to 1 s. Initially, the minipulse nutation angles for DIVAM were set to 7.5°, and the DF pulse angles were fixed at 90°. These angles were chosen for optimum performance for the respective sequences. The DF simulations show that no transverse magnetization builds up, and that all magnetization is restored to the z-axis apart from that which has dephased during the evolution periods. Therefore the degree of loss of z-magnetization depends on the transverse relaxation time in relation to the pulse spacing, and so the degree of selection degrades as the pulse spacing is increased to values on the order of the relaxation time of the magnetizations involved. This is seen in Fig. 5, which shows that as the pulse spacing is increased, the sequence's ability to select for the amorphous signal diminishes. The simulation recovered all the behaviour seen in the experimental data over the whole range of minipulse angles measured. The detailed features in the simulation around 50–60° were not observed in the experimental data, being obscured by the rather high deconvolution noise.

Simulations of the effects of the DIVAM sequence show that even for very fast transverse relaxation times some z-magnetization remains at the end of the minipulse sequence with the parameters given above, since although transverse magnetization is dephased rapidly

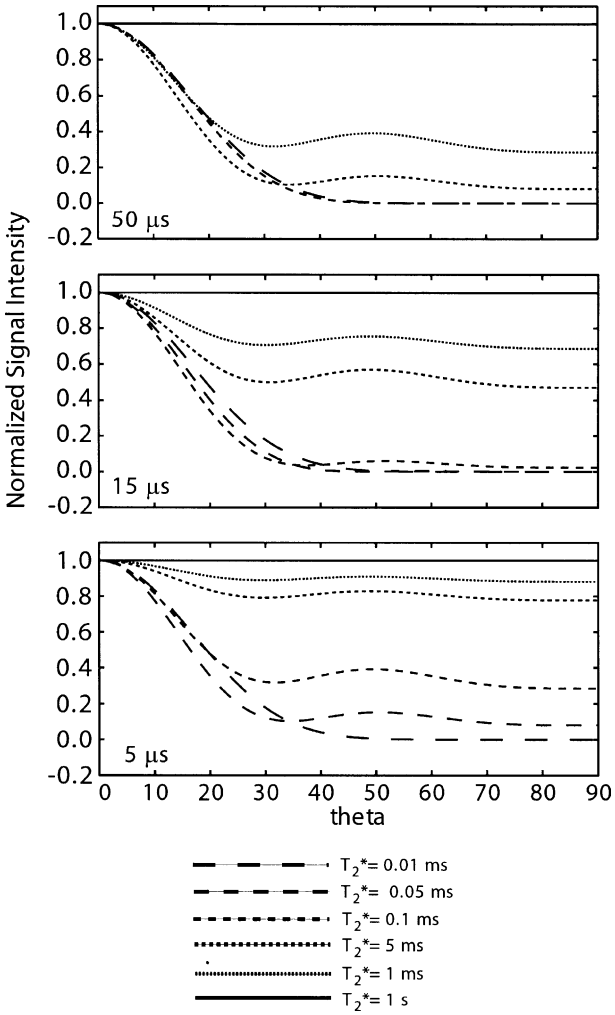

Fig. 7. z-Magnetization at the end of the DP minipulse sequence ($N = 1$) as a function of minipulse nutation angle θ for various values of T_2^*, with T_1 assumed to be 1 s. Three different values of the interpulse time are represented.

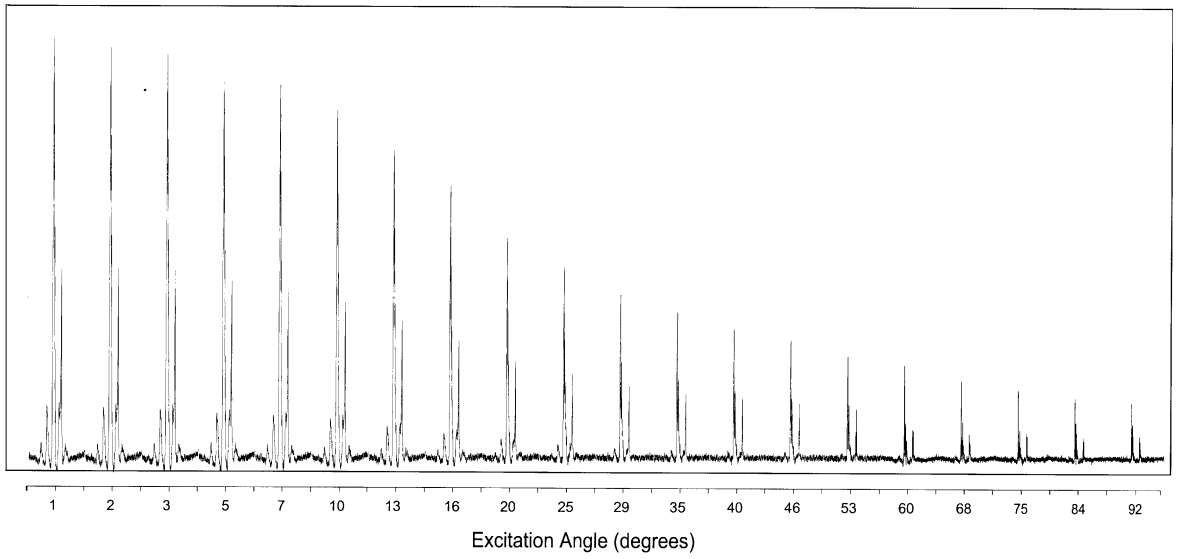

Fig. 8. Experimental spectra for p(VDF/TrFE) under the influence of the DF pulse sequence for a variety of minipulse angles. The interpulse time was 6 μs.

following each minipulse, a 7.5° pulse angle only reduces the z-magnetization by ca. 1%, and no more is lost during the evolution period (τ). For longer relaxation times, less transverse magnetization is dephased during the evolution periods; however, enough occurs to keep the final angle from reaching 90°, leaving residual

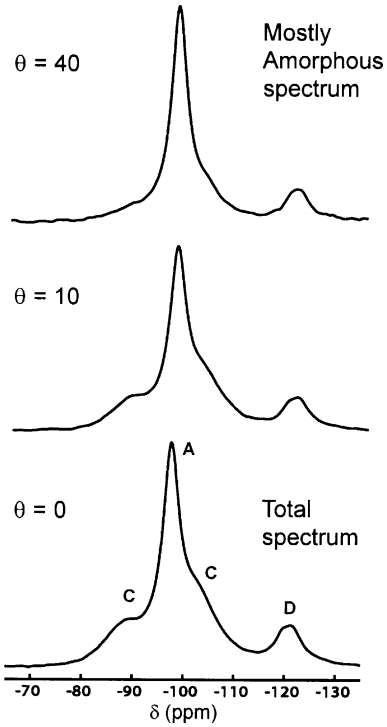

Fig. 9. Spectra of PVDF obtained using the DF pulse sequence for three different minipulse angles, showing the capability of selectivity. The interpulse time was 6 μs. The amorphous, crystalline and defect signals are indicated as A, C, and D, respectively.

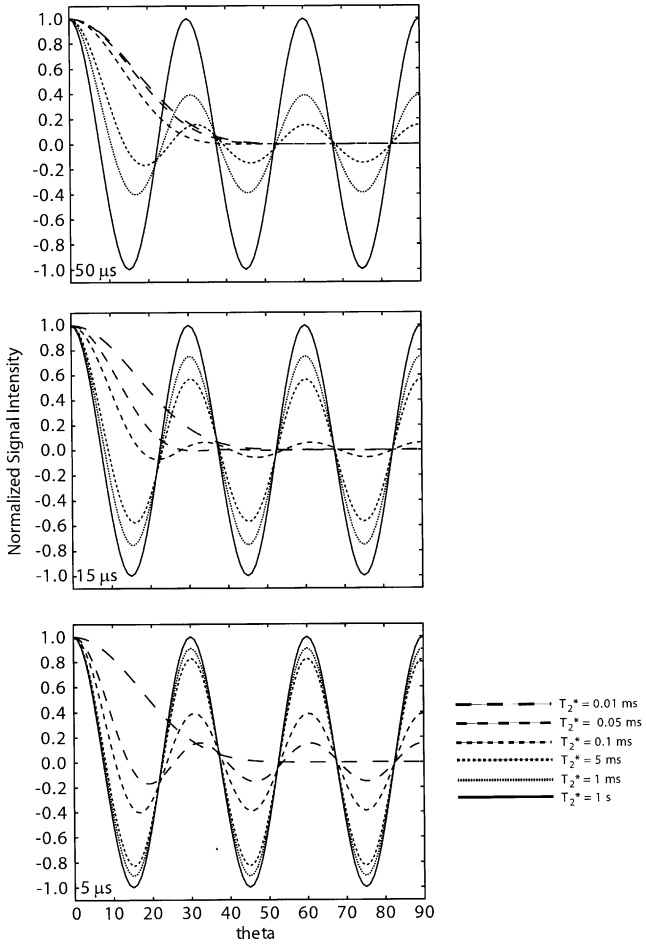

Fig. 10. Simulated plots of z-magnetization for the DIVAM pulse sequence as a function of the minipulse nutation angle for three values of the interpulse time (indicated) and various transverse relaxation times. The longitudinal relaxation time is taken as 1 s.

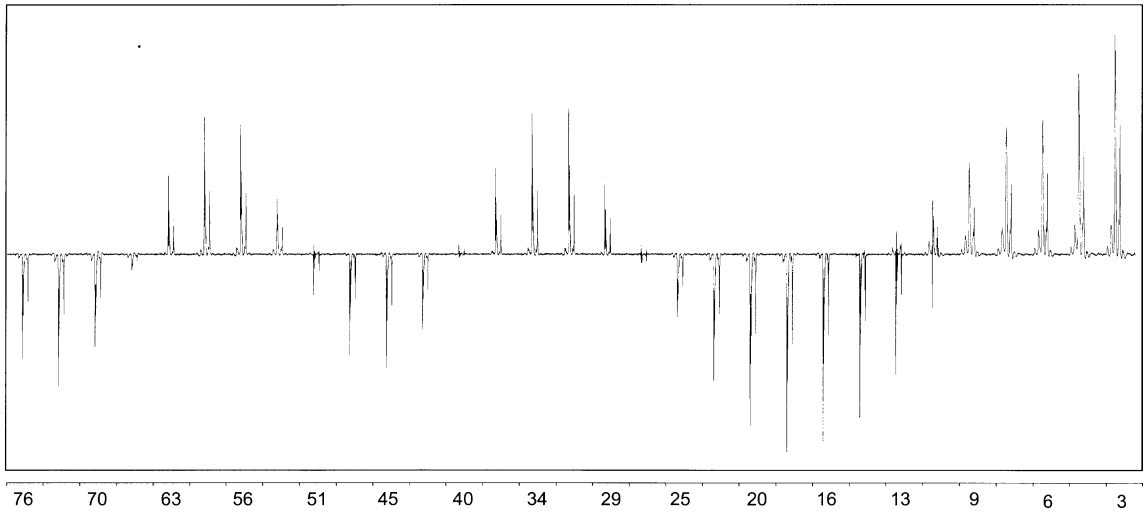

Fig. 11. ^{19}F spectra of p(VDF/TrFE) for the DIVAM pulse sequence as a function of the minipulse nutation angle. The interpulse time was set to 6 μs.

z-magnetization. As the evolution period increases in duration, more dephasing occurs. Thus choosing the correct pulse spacing is of the utmost importance in the experimental design in order to achieve optimum selectivity. Fig. 6 illustrates the selectivity that can be obtained for the amorphous and crystalline domains of PVDF using DIVAM. At the first null situation for the amorphous domain there is still plenty of intensity for the crystalline domain.

Simulations were carried out with variation of the minipulse angles, from 0° to 90° for the DF case with spin–spin relaxation times from 10 μs to 1 s for various pulse spacings (5, 15, and 50 μs). The results are shown in Fig. 7, which therefore shows the degree to which selectivity is obtained between domains differing in T_2^*. In this case the remaining z-magnetization after the 12-pulse train is plotted as a function of the minipulse angle (θ). If no transverse relaxation occurs, the DF sequence returns the magnetization to the z-axis for any value of the excitation angle. The ability to refocus the magnetization diminishes with the degree to which the transverse relaxation distorts the accrued angle of rotation, leaving the final magnetization removed from the z-axis. For small angles θ, the magnetization is not perturbed much, so it stays aligned with the z-axis regardless of the relaxation time. As the angle is increased, the extent of refocusing varies tremendously as a function of both τ and T_2^*. The degree of selectivity of the pulse sequence is optimised for higher angles. Moreover, the relaxation times dictate the pulse spacings to be used for maximising the selectivity. Notice also that one can only select for pure long-T_2^* signals (mobile domains). Even in this case there is usually contamination from some short-T_2^* signal. Experimentally this is shown in Fig. 5, where the optimum selectivity is seen at the larger excitation angles, the optimum pulse spacing is short with

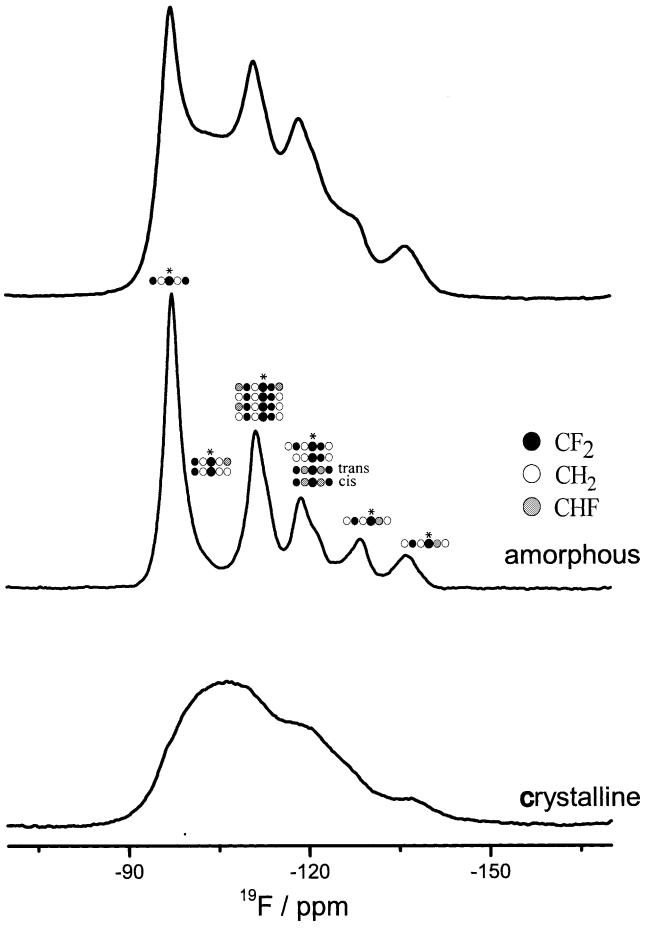

Fig. 12. Fluorine-19 spectra of p(VDF/TrFE) under the influence of the DIVAM pulse sequence, showing the selectivity. Top, full spectrum ($\theta = 0$); Middle, amorphous domain spectrum ($\theta =$ ca. 30°); Bottom, crystalline domain spectrum ($\theta = 7.3°$). In each case the interpulse time was 6 μs. The assignments of the fluorine resonances in the amorphous phase is based on that for the solution phase in [10]. The CF_2 environment giving rise to the signal are indicated by the asterisks.

respect to the T_2^* of the amorphous signal. In each case there is signal present from both magnetizations except when using long pulse spacing. When only amorphous signal is seen, it is significantly diminished in intensity, as also observed in Fig. 8 for the p(VDF/TrFE) copolymer. Fig. 9 illustrates the performance of the DF sequence with various pulse angles for PVDF, where the selection of the amorphous signal improves with increasing pulse angle. In each case, however, there is still residual crystalline signal.

Similar computations were carried out for the DIVAM pulse sequence in which the minipulse angle was varied from 0° to 90°, for spin–spin relaxation times ranging from 10 μs to 1 s and for pulse spacings of 5, 15, and 50 μs, respectively. For long relaxation times the magnetization goes through several rotations in the yz plane with high excitation angles, giving a typically sinusoidal pattern, as seen in Fig. 10. As the relaxation time decreases and minipulse spacing increases, the degree of dephasing in the transverse plane becomes extensive, resulting in the magnetization lagging behind the maximum possible $N\theta$ in net nutation angle θ_t. For very short T_2^*'s it completely dephases before completing the first half cycle. Notice that when the magnetization for long relaxation times (mobile domains) passes through zero for the first time, there is still significant z-magnetization for the magnetization with short relaxation times (rigid domains), thus making it possible to collect signal from just that magnetization.

Fig. 6 shows results for signal intensities of the amorphous and crystalline domains of PVDF separately, as a function of θ for three different values of τ. The simulations fit the observed dependencies rather well. Fig. 11 shows DIVAM spectra of p(VDF/TrFE) copolymer for a series of minipulse excitation angles. A normal MAS spectrum of this semi-crystalline polymer consists of a superposition of crystalline and amorphous subspectra. Upon close inspection of the DIVAM spectra, one can see that the amorphous signal follows the oscillatory pattern, whilst the crystalline signal lags behind and eventually dephases leaving purely amorphous signal. There is a point, however, where the amorphous signal passes through zero but significant crystalline signal remains, which occurs around minipulse angle, θ, of 7.5°. Fig. 12 shows a stacked plot of spectra taken from Fig. 11 at minipulse angles of particular interest. The top spectrum is taken for θ very small, so that no selection takes place, leading to a mixture of amorphous and crystalline signals as expected. The middle spectrum is taken at a large minipulse angle and shows purely amorphous signals. Finally, the bottom spectrum is taken for $\theta = 7.5°$, where the amorphous signal passes through a null, thus yielding purely crystalline signals.

We have also considered the effect of an offset term for the DIVAM sequence, for which the magnetization is allowed to evolve in the transverse plane during the delays between the minipulses. Fig. 13 shows a series of

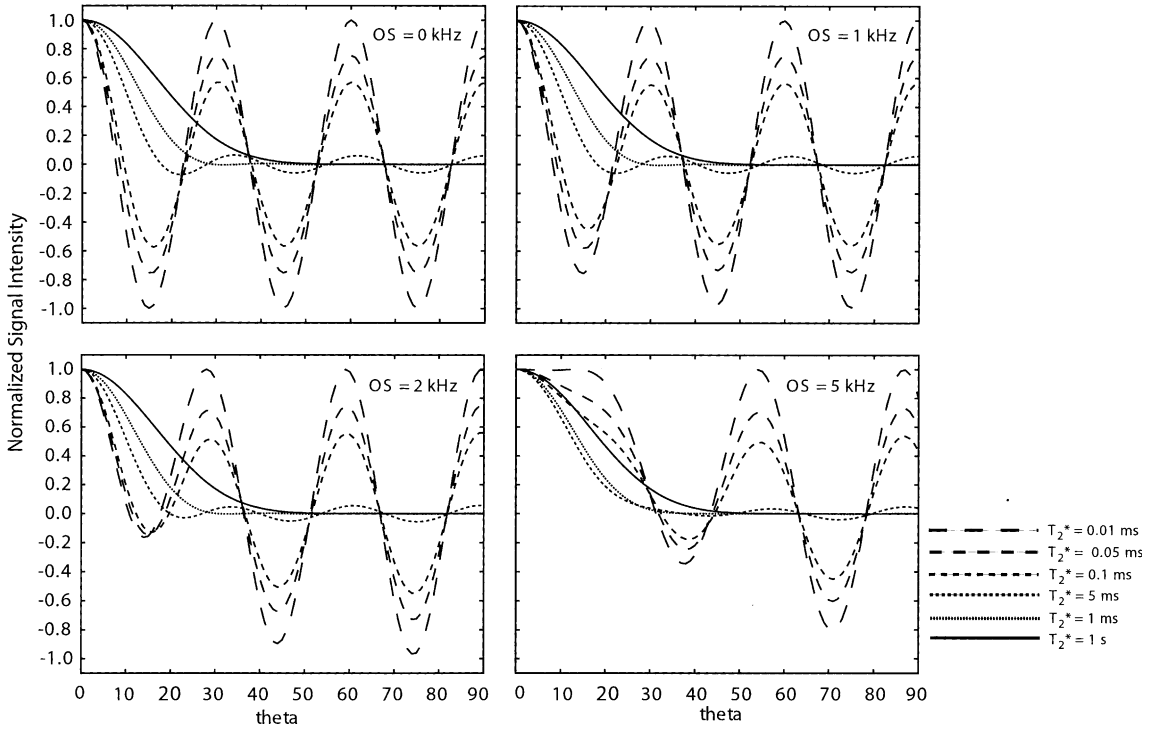

Fig. 13. Simulated plots of z-magnetization for the DIVAM pulse sequence as a function of minipulse nutation angle for increasing offsets from resonance and various transverse relaxation times. The interpulse time was set to 15 μs.

simulations like those in Fig. 10, but for which the offset from resonance is varied from 0 to 5 kHz, for relaxation times ranging from 0.01 ms to 1 s. As the offset frequency increases, those signals with long relaxation times are most effected. Those with short relaxation time seem to dephase before any effect manifests itself. Selection still appears to be possible up to an offset of 2 kHz, with the magnetization with long relaxation times still passing through zero, but significant short-relaxation time signal remains. Eventually, the first null condition is lost, at higher offsets, and the next null occurs when all the short relaxation time signal has completely dephased, making selection impossible.

The off-resonance effect is not as relevant as one would initially anticipate, since offset values in many proton spectra are quite small because of the relatively small chemical shift range of the hydrogen nucleus. In any case, one is interested in selecting signal from highly overlapped lines, so that the offset term is inherently small. These simulations merely give a rough illustration of the situation at hand. More rigorous computations could be performed, including the effects of properly defined dipolar coupling and use of the complete solid-state NMR Hamiltonian under MAS conditions, which will be the subject of a future work.

4. Conclusions

The simulations of z-magnetization resulting from the DF and DIVAM pulse sequences show that in favourable cases the latter can produce separate spectra of crystalline and amorphous domains for semi-crystalline polymers more readily than the former. It is shown that DIVAM can distinguish the two domains for p(VDF/TrFE) with excellent quality and that the simulations can accurately reproduce the results.

Acknowledgments

We are grateful to the UK Engineering and Physical Sciences Research Council for research grant GR/M73514 and for access to the Solid-state NMR Research Service based at Durham. We would also like to acknowledge Philip Wormald for his experimental advice and support.

References

[1] K. Schmidt-Rohr, H.W. Spiess, Multidimensional Solid-State NMR and Polymers, Academic Press, London, 1994.

[2] R.K. Harris, G.A. Monti, P. Holstein, in: S. Ando, T. Asakura (Eds.), ^{19}F NMR Chapter 6.6 of Studies in Physical and Theoretical Chemistry—Solid state NMR of Polymers, Elsevier, Amsterdam, 1998.

[3] E. Hagaman, ^{13}C–^{19}F dipolar dephasing in monofluorinated organic substances. Characterization by ^{1}H–^{13}C–^{19}F triple resonance ^{13}C CP/MAS and ^{19}F MAS NMR, J. Magn Reson. A 104 (1993) 125–131.

[4] N. Egger, K. Schmidt-Rohr, B. Bluemich, W.D. Domke, B. Stapp, Solid state NMR investigation of cationic polymerized epoxy resins, J. Appl. Polym. Sci. 44 (1992) 289–295.

[5] J. Clauss, K. Schmidt-Rohr, A. Adam, C. Boeffel, H.W. Spiess, Stiff macromolecules with aliphatic side chains: side chain mobility, conformation, and organization from 2D solid-state NMR spectroscopy, Macromolecules 25 (1992) 5208–5214;
S. Spiegel, K. Schmidt-Rohr, C. Boeffel, H.W. Spiess, ^{1}H spin diffusion coefficients of highly mobile polymers, Polymer 34 (1993) 4566–4569;
W.Z. Cai, K. Schmidt-Rohr, N. Egger, B. Gerharz, H.W. Spiess, A solid-state n.m.r study of microphase structure and segmental dynamics of poly(styrene-*b*-methylphenylsiloxane) diblock copolymers, Polymer 34 (1993) 267–276;
C. Gyunggoo, A. Natansohn, T. Ho, K.J. Wynne, Phase structure of poly(dimethylsiloxane-ura-urethane)-segmented copolymers as observed by solid-state nuclear magnetic resonance spectra, Macromolecules 29 (1996) 2563–2569;
F. Weingand, D.E. Demco, B. Blumich, H.W. Spiess, Spatially resolved NMR spin diffusion in solid polymers, J. Magn. Reson. A 120 (1996) 190–200;
K. Landfester, C. Boeffel, M. Lambla, H.W. Spiess, Characterization of interfaces in core-shell polymers by advanced solid-state NMR methods, Macromolecules 29 (1996) 5972–5980;
M. Holderle, M. Bruch, H. Luchow, W. Gronski, R. Mulhaupt, Morphology and grafting of oxazoline-functional polymer particles with various carboxylic acids, J. Polym. Sci. Polym. Chem. 36 (1998) 1821–1827;
B. Yan, R. Stark, A WISE NMR approach to heterogeneous biopolymer mixtures: dynamics and domains in wounded potato tissues, Macromolecules 31 (1998) 2600–2605;
M. Marjanski, M. Srinivasarao, P. Mirau, Solid-state multipulse proton nuclear magnetic resonance (NMR) characterization of self-assembling polymer films, Solid State NMR 12 (1998) 113–118;
J.L. White, P. Brant, Direct detection of miscibility in saturated polymer blends, Macromolecules 31 (1998) 5424–5429;
A. Ellwanger, R. Brindle, M. Kaiser, W. Wielandt, E. Linder, K. Albert, *n*-Alkyl fluorenyl phases in chromatography II. Dynamic behaviour and high-performance liquid chromatography applications, J. Chromatogr. A 858 (1999) 133–153;
F. Mellinger, M. Wilhelm, P. Belik, H. Schwind, H.W. Spiess, Quantitative determination of dynamic heterogeneities in coreshell lattices by ^{1}H solid-state NMR, Macromol. Chem. Phys. 200 (1999) 2454–2460;
P. Holstein, G. Monti, R.K. Harris, Proton spin-diffusion in PVDF: a ^{1}H–^{19}F CP/MAS NMR study, Phys. Chem. Chem. Phys. 1 (1999) 3549–3555;
K. Beshah, L. Molnar, Characterization of interface structures and morphologies of heterogeneous polymers: a solid-state ^{1}H NMR study, Macromolecules 33 (2000) 1036–1042;
D.E. Demco, A. Johansonn, J. Tegenfeldt, Proton spin-diffusion for spatial heterogeneity and morphology investigations of polymers, Solid State Nucl. Magn. 4 (1995) 13–38.

[6] S.J. Opella, M.H. Frey, Selection of nonprotonated carbon resonances in solid-state nuclear magnetic resonance, J. Am. Chem. Soc. 101 (1979) 5854.

[7] S. Ando, R.K. Harris, G. Monti, S.A. Reinsberg, Analysis of cross-polarization dynamics between ^{1}H and ^{19}F in Viton fluoroelastomer using solid-state ^{19}F magic angle spinning and ^{1}H–^{19}F

cross-polarization magic angle spinning NMR, Magn. Reson. Chem. 37 (1999) 709–720;
S. Ando, R.K. Harris, S.A. Reinsberg, Analysis of cross-polarization dynamics between two abundant nuclei, ^{19}F and ^{1}H, based spin thermodynamics theory, J. Magn. Reson. 141 (1999) 91–103;
P. Hazendonk, R.K. Harris, G. Galli, S. Pizzanelli, Cross-polarization for a fluoropolymer involving multiple spin baths of abundant nuclei, Phys. Chem. Chem. Phys. 4 (2002) 507–513.

[8] S. Ando, R.K. Harris, P. Holstein, S.A. Reinsberg, K. Yamauchi, Solid-state ^{1}H–$^{19}F/^{19}F$–^{1}H CP/MAS NMR study of poly(vinyl-fluoride), Polymer 42 (2001) 8137.

[9] S. Ando, R.K. Harris, S.A. Reinsberg, Solid-state ^{1}H–$^{19}F/^{19}F$–^{1}H CP/MAS study of poly(vinylidene fluoride), Magn. Reson. Chem. 40 (2002) 97.

[10] P. Mabboux, K. Gleason, ^{19}F NMR characterization of electron beam irradiated vinylidene fluoride–trifluoroethylene copolymers, J. Fluorine Chem. 113 (2002) 27–35.